Solid State Phenomena
ISSN: 1662-9779, Vol. 388, pp 179-185
doi:10.4028/p-l9gdMJ

Submitted: 2026-01-19
Revised: 2026-02-22
Accepted: 2026-02-23
Online: 2026-04-15

Assessing Global and Local Formability from Tensile Tests with Anisotropy Consideration

Guijia Li[1,a] and Junhe Lian[1,b*]

[1]Institute of Metal Forming, RWTH Aachen University, Intzestraße 1, 52072, Aachen, Germany

[a]guijia.li@rwth-aachen.de, [b*]junhe.lian@ibf.rwth-aachen.de

Keywords: formability, anisotropy, failure, fracture, modeling.

Abstract. Medium-Mn steel (MMnS) and quenching and partitioning (QP) steels are two representatives of third-generation advanced high-strength steels (3rd Gen AHSS), developed to achieve an optimal balance between strength and ductility. In forming applications, global formability reflects a material's resistance to necking, while local formability indicates its resistance to fracture. Both aspects are essential for assessing mechanical performance. Global formability is often characterized by forming limit curves at necking and is highly sensitive to work hardening behavior. Similarly, the forming limit curves at fracture determined from different stress states can be applied to evaluate the local formability. In addition, these deformation characteristics can be influenced by anisotropy introduced during sheet processing. Rolling process introduces orientation-dependent variations in both plastic flow and fracture behavior, which significantly affect necking development and fracture initiation. This study investigates and compares the global and local formability of various 3rd Gen AHSS grades, with a focus on the influence of anisotropy. To investigate the anisotropic effects on plasticity and ductile fracture under different stress states, tensile tests were conducted on specimens with various geometries and orientations cut from sheet materials. Based on the tensile tests, the forming limit framework of Shen et al [1] was broadened to include anisotropic effects.

Introduction

Driven by low-carbon design requirements, advanced high-strength steels (AHSS) have been increasingly adopted in automotive body structures to enable lightweight design while maintaining high crashworthiness. Among the newly developed 3rd Gen AHSS, quenching and partitioning (QP) steels and medium-manganese (MMn) steels have attracted particular attention due to their excellent strength-ductility balance and promising application potential. As a trade-off for their strength-ductility synergy, AHSS exhibits forming limits and failure behaviors that differ from those of conventional sheet metals, these characteristics play a decision role in the forming process. To better characterize the formability of AHSSs, Heibel et al. [2] introduced the concepts of global formability and local formability, providing a more comprehensive framework for interpreting deformation and fracture behaviors in sheet forming. Shen et al. [1] proposed a unified forming limit framework by integrating three distinct failure criteria including necking, ductile fracture and cleavage fracture, which allows for a direct and intuitive visualization of the competitive relationship among the different failure mechanisms. Global formability describes the ability to undergo uniform deformation without the onset of necking and is commonly characterized by the forming limit curve (FLC). The FLC may be obtained either from experiments, such as Nakajima test, or from theoretical calculations based on the modified maximum force criterion (MMFC) [3] or other models, including the MK model [4]. In contrast, local formability refers to the ability of a material to undergo plastic deformation in a local area without fracture. It is often assessed through hole expansion or bending tests in which the hole expansion ratio is measured as a representative metric [5]. Another effective way to characterize local formability is through local measurements of fracture strain, which are commonly employed in damage models and fracture criteria [2].

It is important to note that both global and local formability are strongly governed by the underlying stress state, which in turn is significantly influenced by material anisotropy in sheet metals.

Anisotropy originates from crystallographic texture, phase morphology, and thermomechanical processing history, and manifests not only in yielding and hardening behavior, but also in strain localization, damage evolution, and fracture, particularly under complex stress states typical of sheet metal forming operations. For AHSS, recent studies have revealed both plastic anisotropy and fracture anisotropy [6], which have been shown to strongly affect necking behavior, fracture mechanisms, and the resulting forming limits. In QP steels, the presence of multiphase microstructures and deformation-induced transformation of retained austenite further complicates the manifestation of anisotropy, leading to a strong dependence of deformation and fracture behavior on loading direction and stress state. Consequently, anisotropy plays a critical role in determining both global and local formability. Although the anisotropic plasticity and fracture behavior of QP steels have received increasing attention in recent years, most existing studies focus on individual material grades or specific loading paths. As a result, few studies have employed a unified framework to systematically and comprehensively evaluate the anisotropy sensitivity of formability across different grades of QP steels.

In this work, the anisotropy sensitivity of both global and local formability is systematically investigated for multiple QP steel grades within a unified forming limit framework. By combining necking- and fracture-based formability metrics under different stress states, the interplay between anisotropy, strain localization, and fracture is quantitatively assessed, providing new insights into the formability design and material selection of QP steels for advanced sheet metal forming applications.

Material and Experiments

Three as-received high-strength QP steels (QP1000, QP1200 and QP1400) and one MMn steel (MMnS1000) were studied in this work. The mechanical testing program applied by Li et al. [6] was applied to investigate the anisotropic plastic flow properties and fracture properties. Both properties were characterized by uniaxial tensile tests conducted at room temperature under quasi-static loading conditions. While plastic behavior was assessed using standard dog-bone (SDB) specimens, fracture behavior was examined using a set of specially designed specimens, including notched dog-bone (NDB), central hole (CH), and simple shear (SH) geometries. Different specimen geometries and loading configurations were employed to cover a wide range of stress triaxialities, enabling an assessment of both global and local formability. These geometries (as shown in Fig. 1) were adopted from previously validated designs and optimized to ensure stable fracture initiation within the gauge region [6]. To capture anisotropy, all specimens were machined by electrical discharge machining (EDM) along the rolling (RD), diagonal (DD), and transverse (TD) directions.

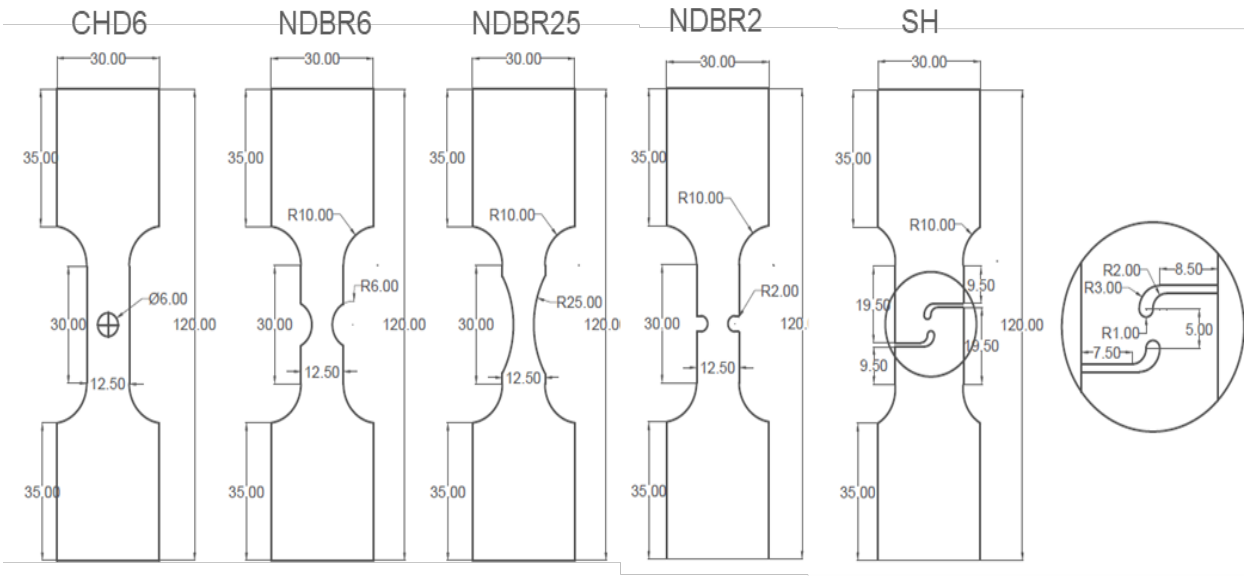

Fig. 1. The sketches of fracture specimen geometries with dimensions.

A stereo digital image correlation (DIC) system was employed during the uniaxial tensile tests to measure full-filed surface strain distributions. The DIC measurements were primarily used to characterize the anisotropy of plastic deformation. It should be noted that the fracture strain was not determined from DIC results in this study. One reason is that DIC measurements are limited to surface strains and therefore cannot fully capture the through-thickness deformation and damage evolution associated with fracture initiation. In addition, DIC data alone does not allow for an unambiguous determination of the local stress states. Consequently, the fracture strain and stress states were determined using finite element simulation, in which the stress and strain states at fracture initiation were identified. The numerical modeling approach is described in detail in next section.

As a basis for subsequent analysis of anisotropy and formability, the plastic deformation behavior obtained from uniaxial tensile tests is first examined. Fig. 2a presents the true stress-effective plastic strain curves together with the corresponding strain hardening rates for the investigated AHSS grades, including QP1000, QP1200, QP1400, and MMnS1000. With increasing strength level, the QP steels exhibit higher flow stresses accompanied by a reduced uniform plastic deformation capacity. In contrast, MMnS1000 shows a lower strength level but a markedly extended strain hardening capacity, resulting in a larger attainable plastic strain. The evolution of the r-value with strain was observed obviously for these materials, as shown in Fig. 2b-d. In particular, MMnS1000 exhibits the most pronounced fluctuation in r-values, which is attributed to its highest degree of phase transformation. Plastic anisotropy is evident for all materials, as reflected by the distinct stress-strain response along RD and TD. More importantly, the intersection between the true stress curve and the corresponding strain hardening rate curve provides a rough measure of the onset of uniform deformation instability, according to the Considère criterion. This intersection defines the maximum uniform strain, in another word, the onset of localized necking. Pronounced directional differences in this critical strain are observed among the investigated steels, indicating that anisotropy manifests primarily through variations in necking limit rather than through differences in flow stress alone. For each material, the maximum uniform strain in the transverse direction (TD) is smaller than that in the rolling direction (RD). This observation suggests that global formability is reduced in TD, reflecting a pronounced directional dependence of the necking limit.

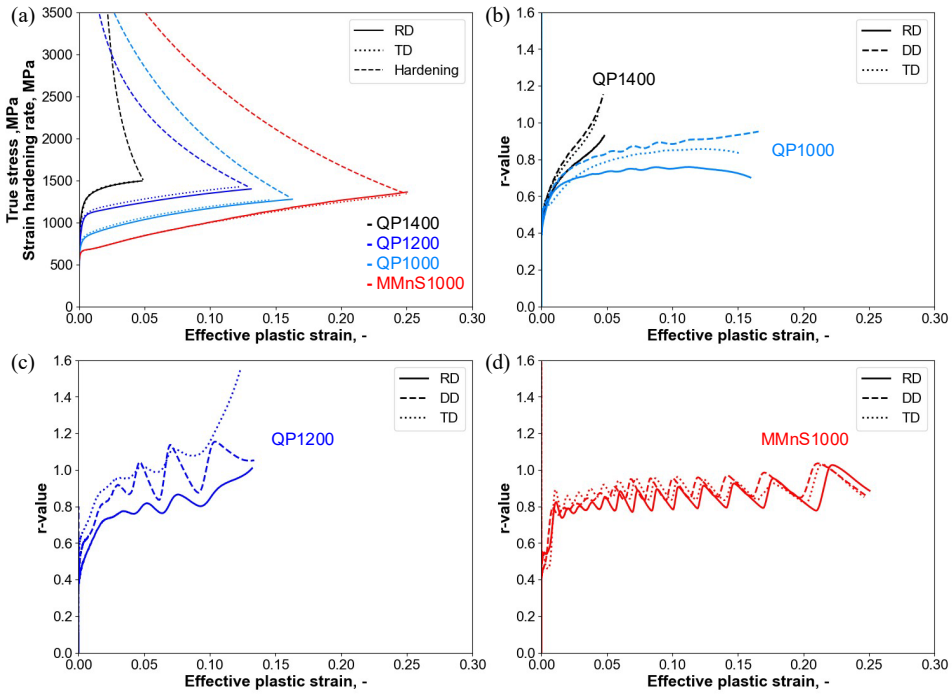

Fig. 2. Mechanical response of the materials investigated. (a)True stress-strain curves in RD and TD and strain hardening rates for RD; evolution of r-values with increasing plastic strain in RD, DD, and TD for four (b) QP1400 and QP1000, (c) QP1200, and (d) MMnS1000.

Numerical Modeling

Localized deformation is a dominant failure mode that limits the global formability of ductile sheet metals. In this study, the forming limit at the onset of localized necking is predicted using the modified maximum force criterion (MMFC). The MMFC extends the classic Considère criterion by accounting for the evolution of the strain path during deformation. While the Considère criterion assumes a constant strain path and predicts instability when the true stress equals the strain hardening rate under uniaxial tension, experimental observation indicate that the local stress state progressively evolves toward plane-strain tension as deformation proceeds beyond the uniform stage. Within the MMFC framework, the strain path is described by the strain increment ratio β and the stress ratio α, which characterize the deformation mode under plane stress conditions. When von Mises plasticity is assumed, these two variables are uniquely related, allowing the strain path evolution to be explicitly determined. The onset of localized necking is identified when the MMFC condition is satisfied, yielding the critical equivalent plastic strain corresponding to the forming limit at necking. Under plane stress conditions relevant to sheet metal forming, the stress ratio α can be further related to stress triaxiality and the Lode angle parameter. Consequently, the predicted forming limit can be expressed as a function of stress state parameters, enabling a consistent assessment of global formability across different loading conditions. In the present work, the MMFC is implemented within an anisotropy plasticity model enHill48 proposed by Lian et al [7]. Since the plasticity model is changed from von Mises to enHill48, the relationship between the strain increment ratio β and the stress ratio α in the MMFC formulation changes accordingly. The detailed mathematical derivation is available in Lian et al [7].

While global formability is governed by the onset of localized necking, local formability is controlled by damage accumulation and fracture under localized deformation. In order to characterize the fracture-dominated forming limits, local formability is assessed in this work using a stress-state-dependent fracture model, namely the MBW fracture model [8]. The MBW model describes fracture initiation in terms of a fracture locus expressed as a function of stress state parameters, η_{avg} and $\bar{\theta}_{avg}$, enabling a quantitative prediction of fracture strain under different loading conditions. The four parameters $F_1 \sim F_4$ in the MBW model are calibrated using a combined experimental and numerical approach based on fracture tests conducted on specimens with different geometries, including notched dog-bone (NDB), central hole (CH), and simple shear (SH). The fracture displacement measured experimentally is coupled with finite element simulations to identify the corresponding fracture strain and stress state at the onset of fracture. This hybrid calibration strategy enables consistent determination of the fracture locus across a wide range of stress states. To avoid excessive complexity in the overall modeling framework, anisotropy in fracture behavior was accounted for by calibrating the MBW fracture parameters separately for each orientation. A fully anisotropic MBW fracture model was therefore not introduced in the present study. This approach allows the directional dependence of fracture behavior to be captured in an effective manner while maintaining a manageable modeling complexity.

$$\bar{\varepsilon}_{df}^{P}\left(\eta_{avg}, \bar{\theta}_{avg}\right) = \begin{cases} +\infty & \eta_{avg} \le \eta_c \\ (F_1 exp^{-F_2\eta_{avg}} - F_3 exp^{-F_4\eta_{avg}})\bar{\theta}^2 + F_3 exp^{-F_4\eta_{avg}} & \eta_{avg} > \eta_c \end{cases} \quad (1)$$

Prior to the fracture modeling, a non-associated anisotropic plasticity model was calibrated to enable reliable finite element simulations. In the present work, the enHill48 yield function was adopted to describe the anisotropic plastic behavior of the investigated materials. The parameters of the enHill48 model were identified using the stress strain responses and corresponding r values obtained from SDB tensile tests conducted along the RD, DD and TD. By fitting these curves, the enHill48 model captures not only the directional dependence of plastic flow but also the evolution of anisotropy with strain increasing. The detailed formulation of the enHill48 model and its calibration procedure are omitted in this paper and can be found in Lian et al [7].

Results and Discussion

As a first step, the experimental true stress strain curves obtained from uniaxial tensile tests were fitted using Swift-Voce hardening law, as shown in Fig. 3(a). The fitted curves, obtained through FEM based optimization, show good agreement with the experimental data over the relevant strain range, providing a sound basis for the subsequent MMFC numerical calculations. By tracking the evolution of stress and strain according to the MMFC criterion, the critical strains corresponding to necking were identified for different strain paths. The resulting limit curves expressed in the principal strain space are presented in Fig. 3(b). The predicted FLCs provide a quantitative description of global formability and allow for a direct comparison between different AHSS grades and different orientations. It is evident that the FLC of MMnS1000 is higher than those of the three QP steels. Moreover, among the QP steels, the predicted FLCs decrease with increasing strength level. This trend is consistent with the well-established understanding that higher material strength is generally accompanied by reduced formability. Regarding the anisotropy of FLCs, only minor differences between RD and TD are observed for all materials, indicating a relatively weak directional dependence of global formability.

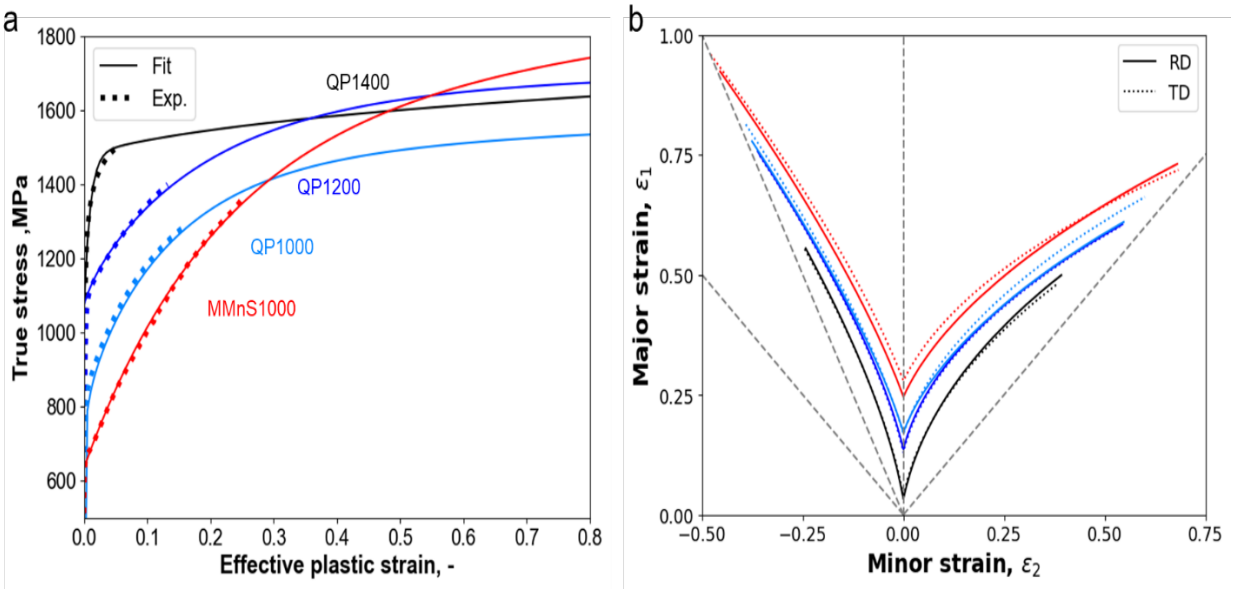

Fig. 3. (a) Fitting of the experimental true stress strain curves using Swift-Voce hardening law; (b) FLC in the principal strain space predicted by the MMFC criterion based on the fitted hardening behavior.

With optimized hardening law calibrated from the uniaxial tensile tests, FEM was performed to reproduce the deformation and fracture process of the investigated specimens. By combining the FEM results with the experimentally measured fracture displacement, the fracture strain at the onset of fracture was identified together with the corresponding stress state and its evolution over the entire deformation history. Fig. 4 presents the local formability of QP1000 in terms of fracture locus and corresponding fracture limit curves. Fig. 4(a) shows the fracture locus expressed as equivalent fracture strain as a function of stress triaxiality under plane stress conditions. The results are obtained using the calibrated MBW fracture model and are illustrated together with the stress state evolution paths associated with different fracture specimen geometries. Fig. 4(b) presents the transformation of the plane stress fracture locus into the principal strain space. The resulting fracture forming limit curve (FFL) is plotted together with the forming limit curve (FLC) presenting global formability, enabling a direct comparison between necking- and fracture-controlled limits. The comparison highlights the stress-state-dependent nature of local formability and its interaction with global formability under plane stress conditions. In addition, the strain paths corresponding to different specimen geometries are also shown.

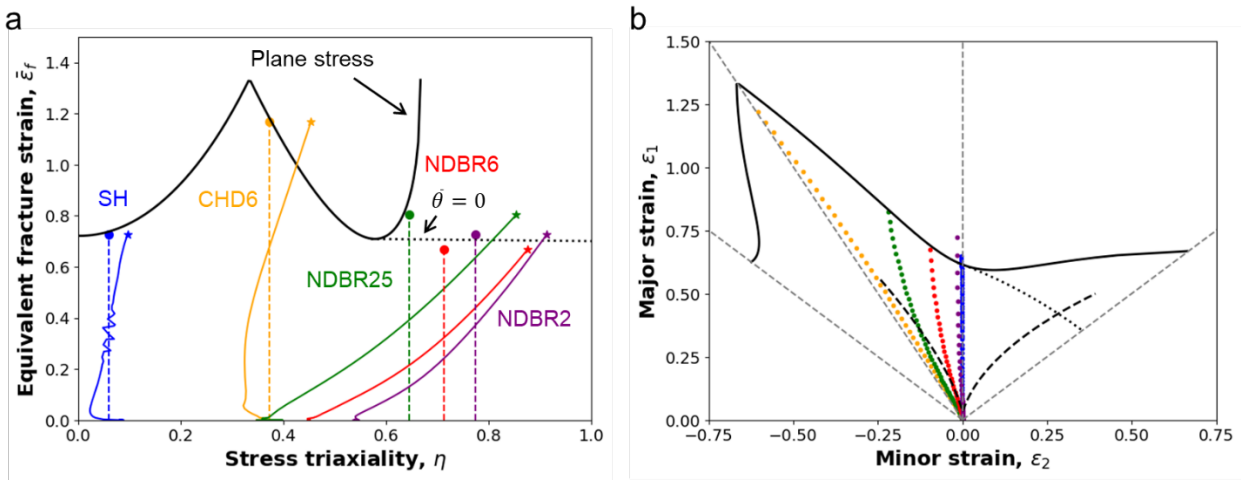

Fig. 4. (a) Fracture locus from calibrated MBW model of QP1000 and the stress states evolution for different geometries; (b) fracture limit curve in the principal strain space and strain path for different geometries.

The same experimental-numerical procedure was subsequently applied to the other investigated materials, including QP1200 and QP1400, to enable a consistent comparison of both global and local formability as well as a comparison between different QP steel grades. Fig. 5 summarizes the predicted forming and fracture limits for the different QP steel grades in both the principal strain space and the stress-state space. First, pronounced directional differences are observed in the fracture limit curves, for all investigated materials. In general, the local formability along RD is consistently higher than that of TD and this is particularly evident in the fracture limit curves of QP1000. Second, the comparison among different materials reveals an interesting trend in global and local formability. With increasing strength leave, the gap between the global and local forming limit curves becomes progressively larger. In some stress state regions of QP1000 and QP1200, fracture occurs after the onset of necking, resulting in a local forming limit curve that is higher.

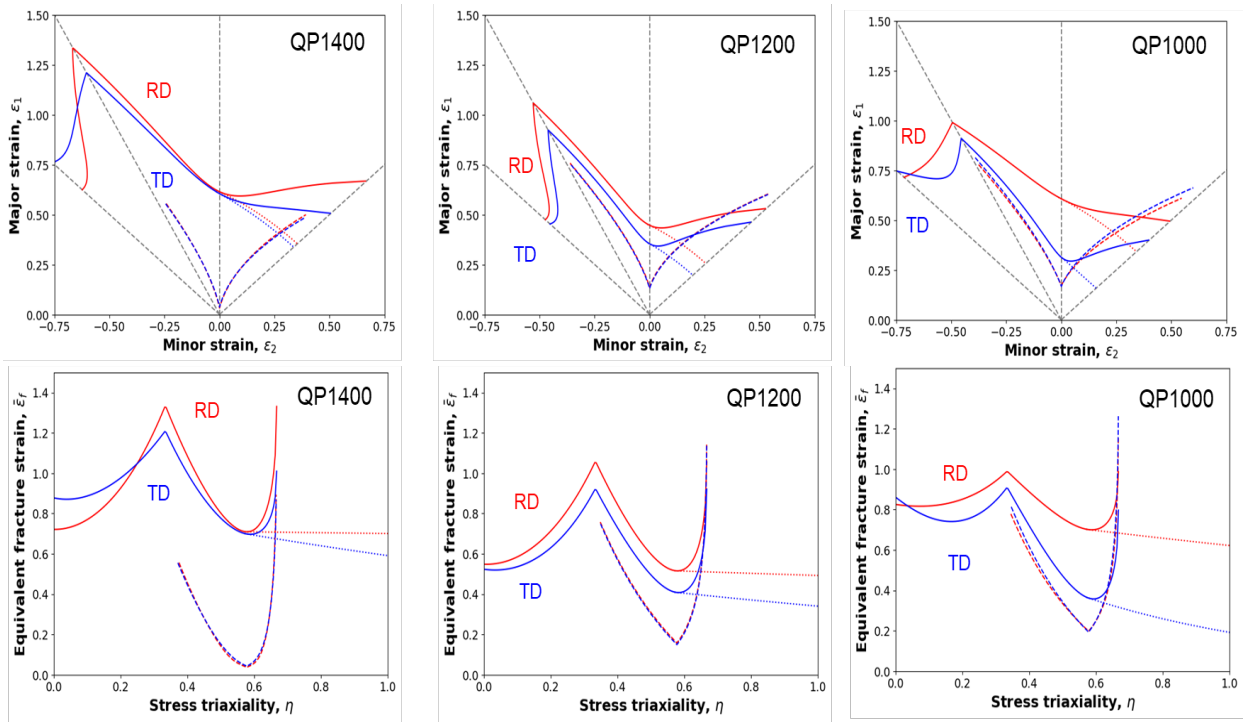

Fig. 5. Comparison of global and local formability for three QP steels along two orientations based on FFL and FLC separately.

Summary

This work investigates the global and local formability of three QP steels (QP1000, QP1200, and QP1400) and one medium-Mn steel (MMnS1000), with a focus on the influence of anisotropy. A unified experimental–numerical framework combining uniaxial tensile tests and finite element simulations was employed to evaluate necking- and fracture-controlled forming limits under different stress states and material orientations.

Global formability was assessed using forming limit curves (FLCs) predicted by the modified maximum force criteria (MMFC) based on FEM-calibrated hardening laws. The results show that MMnS1000 exhibits higher global formability than the QP steels, while the FLCs of QP steels decrease with increasing strength level. Directional differences in global formability between rolling and transverse directions are relatively small.

Local formability was characterized by fracture limit curves (FFLs) obtained from a stress-state-dependent MBW fracture model calibrated using a combined experimental–numerical approach. In contrast to global formability, local formability exhibits pronounced directional anisotropy, with consistently higher fracture limits along the rolling direction. Among the QP steels, QP1000 shows the strongest directional dependence.

A direct comparison between global and local forming limits reveals an increasing separation between necking- and fracture-controlled limits with increasing strength level. For QP1000 and QP1200, local forming limits exceed global forming limits in certain stress-state regions, indicating a transition in the dominant failure mechanism.

References

[1] F. Shen, Y. Sparrer, J. Rao, M. Könemann, S. Münstermann, and J. Lian, “A forming limit framework accounting for various failure mechanisms: Localization, ductile and cleavage fracture,” *Int. J. Plast.*, vol. 175, p. 103921, Apr. 2024, doi: 10.1016/j.ijplas.2024.103921.

[2] S. Heibel, T. Dettinger, W. Nester, T. Clausmeyer, and A. E. Tekkaya, “Damage Mechanisms and Mechanical Properties of High-Strength Multiphase Steels,” *Materials*, vol. 11, no. 5, p. 761, May 2018, doi: 10.3390/ma11050761.

[3] P. Hora, L. Tong, and B. Berisha, “Modified maximum force criterion, a model for the theoretical prediction of forming limit curves,” *Int. J. Mater. Form.*, vol. 6, no. 2, pp. 267–279, Jun. 2013, doi: 10.1007/s12289-011-1084-1.

[4] Z. Marciniak and K. Kuczyński, “Limit strains in the processes of stretch-forming sheet metal,” *Int. J. Mech. Sci.*, vol. 9, no. 9, pp. 609–620, Sep. 1967, doi: 10.1016/0020-7403(67)90066-5.

[5] F. Shen *et al.*, “Local formability of medium-Mn steel,” *J. Mater. Process. Technol.*, vol. 299, p. 117368, Jan. 2022, doi: 10.1016/j.jmatprotec.2021.117368.

[6] Z. Li *et al.*, “Anisotropic fracture behavior of the 3rd generation advanced high-strength – Quenching and Partitioning steels: Experiments and simulation,” *J. Mater. Res. Technol.*, vol. 30, pp. 9395–9414, May 2024, doi: 10.1016/j.jmrt.2024.05.228.

[7] J. Lian *et al.*, “An evolving non-associated Hill48 plasticity model accounting for anisotropic hardening and r-value evolution and its application to forming limit prediction,” *Int. J. Solids Struct.*, vol. 151, pp. 20–44, Oct. 2018, doi: 10.1016/j.ijsolstr.2017.04.007.

[8] J. Lian, M. Sharaf, F. Archie, and S. Münstermann, “A hybrid approach for modelling of plasticity and failure behaviour of advanced high-strength steel sheets,” *Int. J. Damage Mech.*, vol. 22, no. 2, pp. 188–218, Mar. 2013, doi: 10.1177/1056789512439319.

The publication of this article was funded by the RWTH Aachen University 10.13039/501100007210